JOURNAL OF GEOPHYSICAL RESEARCH, VOL. 104, NO. C8, PAGES 18,447–18,461, AUGUST 15, 1999

Waves and currents over a fixed rippled bed
3. Bottom and apparent roughness for spectral waves and currents

Paul Peter Mathisen

Department of Civil and Environmental Engineering, Worcester Polytechnic Institute, Worcester, Massachusetts

Ole Secher Madsen

Ralph M. Parsons Laboratory, Department of Civil and Environmental Engineering
Massachusetts Institute of Technology, Cambridge

Abstract. This paper is the third in a series of three that presents the results of experiments designed to verify the use of a single bottom roughness length scale for waves and currents over a rough bed. While the first two papers concentrated on the bottom roughnesses experienced by monochromatic wave and current boundary layer flows, this paper presents the results of additional experiments that investigate the use of an equivalent wave representation to extend these results to spectral wave and current boundary layer flows. Spectral waves, simulated by five components, and currents were generated in a 20-m-long wave flume with a fixed rippled bottom. Attenuation due to bottom friction is determined from total attenuation measurements for individual wave components by removing the effects of sidewall dissipation and wave-wave interactions. These attenuation estimates are used to establish representative friction factors, which are used in conjunction with an existing eddy viscosity model to determine bottom roughnesses. The bottom roughnesses experienced by spectral waves (in the presence and absence of a current) match the bottom roughnesses for monochromatic waves. When these experimentally determined bottom roughnesses are used in conjunction with the eddy viscosity model, predictions of attenuation for individual wave components closely match measurements. When the wave boundary layer thickness is defined to be the height at which the predicted velocity deficit in the wave boundary layer is within 5% of the free stream velocity, excellent agreement is obtained between predicted and measured velocity profiles for currents in the presence of codirectional waves. Therefore these experiments show that a single bottom roughness, when used in conjunction with an equivalent wave representation, adequately characterizes both monochromatic and spectral wave-current boundary layer flows over a fixed rippled bed.

1. Introduction

Fluid velocities in bottom boundary layers play a significant role in defining circulation and sediment transport in coastal regions. Accordingly, numerous investigators have developed models to predict velocity distributions in bottom boundary layers for waves and currents. The most widely used models achieve turbulence closure using an eddy viscosity because of the simplicity and utility of this approach. To scale the eddy viscosity near the bottom, most eddy viscosity models use a time-invariant shear velocity for a velocity scale and the distance from the bed for the length scale. Examples of these eddy viscosity models include the models of *Lundgren* [1972], *Smith* [1977], *Tanaka and Shuto* [1981], *Christoffersen and Jonsson* [1985], and *Grant and Madsen* [1979, 1986]. In particular, the model of *Grant and Madsen* [1979, 1986] defines separate forms of the eddy viscosity for the regions inside and outside the wave boundary layer. A shear velocity based on the shear stress experienced by the current defines the velocity scale above the wave boundary layer, and a shear velocity based on the maximum combined bottom shear stress defines the velocity scale for the region within the wave boundary layer. Using this approach, *Grant and Madsen* [1979, 1986] developed solutions for the profiles associated with the wave velocity and time-averaged current velocity.

All these eddy viscosity models assume that the effects of the bottom on velocity profiles for waves and/or currents can be represented in terms of a single roughness length scale k_n. However, the validity of this assumption is not intuitively obvious in light of the different characteristics of fluid–bed form interactions observed under pure currents and pure oscillatory motion. Therefore *Mathisen and Madsen* [1996a, b] addressed the validity of this assumption using experiments with periodic or monochromatic waves over a fixed rippled bed in a wave flume. These experiments made use of a piston-type wave maker and current generation system to generate wave and current boundary layer flows in a 20-m-long wave flume with 1.5-cm-high triangular bars placed at 10-cm intervals along the bottom to simulate ripples. *Mathisen and Madsen* [1996a] measured wave attenuation and used the eddy viscosity model of *Grant and Madsen* [1986] to determine roughnesses experienced by the waves (i.e., wave roughnesses) in the presence

Paper number 1999JC900114.
0148-0227/99/1999JC900114$09.00

and absence of a current. *Grant and Madsen* [1986] related the bottom roughness to the wave friction factor by using the velocity gradient to evaluate the magnitude of the wave shear stress, $|\tau(t)|$, at an elevation of $z = 0$ and neglecting any phase difference between the bottom shear stress and near-bottom velocity, $u(t)$. *Mathisen and Madsen* [1996a] found that, when the shear stress is evaluated at the hydraulic roughness height ($z_o = k_n/30$) and the analysis of *Grant and Madsen* [1986] is modified to account for the phase difference between the bottom shear stress and near-bottom horizontal orbital velocity, the roughnesses for waves matched the roughnesses for pure currents flowing over the same bed.

The *Grant and Madsen* [1986] model can also be used to predict a logarithmic time-averaged velocity profile outside of the wave boundary layer. The nature of this outer velocity profile is typically defined in terms of a current shear velocity and an apparent hydraulic roughness that accounts for the effects of the bottom roughness and wave-current interaction within the wave boundary layer. *Mathisen and Madsen* [1996b] estimated the bottom and apparent roughness using time-averaged velocity profiles measured for currents in the presence of waves. These analyses showed that the predictions afforded by the *Grant and Madsen* [1986] model underpredicted the apparent roughnesses experienced by the current. The difference was shown to be the result of an underprediction of the wave boundary layer thickness as well as a steady streaming induced by the wave motion. By modifying the wave boundary layer thickness and using data from pure wave experiments to estimate the wave-induced mass transport, the bottom roughnesses for pure current, pure wave, and combined wave and current boundary layer flows were shown to be the same.

The vast majority of the eddy viscosity models (including all models cited previously) assume that the wave field consists of simple periodic waves. Consequently, the experiments of *Mathisen and Madsen* [1996a, b] served to verify the use of a single bottom roughness when applied for simple periodic waves in accordance with the eddy viscosity model of *Grant and Madsen* [1986]. It is well known, however, that the wave climate in the coastal environment is commonly dominated by random or irregular waves with a range of amplitudes, frequencies, and directions. The properties of near-bottom interactions for these random waves will be different from the near-bottom characteristics for monochromatic waves. For example, as monochromatic waves pass over a rippled bed, eddies would be expected to develop on the leeside of the ripples during every wave cycle as wave crests (and troughs) pass by. However, as spectral waves pass over a rippled bed, the random nature of the wave field leads to the formation of eddies on the leeside of ripples that are also random in nature. The random nature of these eddies is closely related to the random nature of near-bottom horizontal velocities owing to the superposition of individual wave components. Since the development of these eddies has an important effect on energy dissipation in the bottom boundary layer, it is not clear that the roughness experienced by spectral waves would be the same as that of monochromatic waves. Furthermore, no previous experiments have been conducted that can be used to verify that a single roughness can characterize boundary layers for monochromatic and spectral waves.

In addition to routinely representing the bottom in terms of a single roughness scale, investigators have also commonly represented random wave fields in terms of a single representative monochromatic wave, which provides an approach for extending the application of monochromatic wave models to random wave fields. A variety of formulations have been used to define this representative monochromatic wave for a given wave spectrum [e.g., *U.S. Army Coastal Engineering Research Center*, 1984]. The application of the equivalent wave concept to characterize wave attenuation in the bottom boundary layer of spectral waves was first addressed extensively by *Hasselmann and Collins* [1968]. *Collins* [1972] expanded upon this earlier work and defined an equivalent wave representation by equating its root-mean-square (rms) near-bottom horizontal orbital velocity amplitude to the rms amplitude for the near-bottom orbital velocity spectrum. *Madsen et al*. [1988] developed a theoretical spectral dissipation model that related the friction factor to the bottom roughness for pure spectral waves. *Madsen* [1994] showed from theoretical considerations that the definition of an equivalent wave based on the rms horizontal orbital velocity is appropriate for boundary layers. Accordingly, by making use of the equivalent wave, *Madsen* [1994] was able to extend the underlying concepts of the *Grant and Madsen* [1986] model to spectral wave and current boundary layer flows. However, no laboratory or field experiments have provided data to confirm that this equivalent wave representation can be used to represent the characteristics of spectral wave and current boundary layer flows.

The primary objective of this paper is to show that the bottom roughness length scale for monochromatic waves propagating over a fixed bed may be used in conjunction with an equivalent wave representation to characterize boundary layers for pure spectral wave and spectral wave-current flows over the same bottom configuration. This objective is satisfied using a series of experiments with spectral wave and current flows generated in the same flume as the flume used for the experiments of *Mathisen and Madsen* [1996a, b]. Since the experiments as well as the theoretical model of *Madsen* [1994] provide estimates of wave attenuation for individual frequencies in a spectrum, this paper also addresses the prediction of wave attenuation for different spectral frequencies. Accordingly, this paper compliments those of *Mathisen and Madsen* [1996a, b] by presenting the results of additional experiments in this same wave flume to extend the monochromatic wave results of those papers to the more realistic case of spectral wave and current boundary layer flows.

Roughnesses experienced by the waves (i.e., wave roughnesses) are determined by analyzing wave attenuation measurements, and roughnesses experienced by the current (i.e., current roughnesses) are determined by analyzing time-averaged velocity profiles. Section 2 provides a brief description of the experimental setup and a discussion of the selection of an eddy viscosity model for use in this analysis. Section 3 describes the procedures for using a discrete wave spectrum to approximate a continuous wave spectrum, and section 4 summarizes the use of wave surface profile measurements to determine wave attenuation due to bottom friction. Section 5 presents the use of these attenuation data to determine values for the pure wave roughness, k_w, and wave roughness in the presence of a current, k_{wc}, and section 6 discusses the use of the *Madsen* [1994] model to predict attenuation for individual wave components. Finally, section 7 presents comparisons between measured and predicted time-averaged velocity profiles and their interpretation in terms of the apparent hydraulic roughness experienced by the current, z_{oa}. This section also includes an alternative approach in which the measured apparent roughnesses are used as input to the *Madsen* [1994] model to provide independent estimates for the bottom roughness for the current in the presence of waves, k_{cw}.

2. Experimental Approach

2.1. Experimental Setup

The spectral waves and currents were generated in a 20-m-long by 0.90-m-deep by 0.76-m-wide flume equipped with a piston-type programmable wave maker and a current generation system. A low-powered (20 mW), single-axis laser Doppler anemometer was used to measure time-averaged velocity profiles, and resistance-type wave gauges were used to measure wave characteristics. As discussed by *Mathisen and Madsen* [1996a], the magnitudes of the bottom roughnesses are affected by bed form geometry, near-bottom flow characteristics, or a combination of both. Therefore all experiments make use of a single, fixed bed form geometry in order to isolate the effects of near-bottom flow characteristics on the bottom roughness. Rough turbulent boundary layers were generated using 1.5-cm-high triangular bars placed at 10-cm intervals along the bottom of the flume. Since all bars extended across the width of the flume, the bars acted as strip roughness elements that simulate bottom bed forms or ripples. This bottom configuration is the same as that used for the majority of the monochromatic wave experiments of *Mathisen and Madsen* [1996a, b]. The bottom configuration also closely matches the characteristics of ripples analyzed by *Mathisen* [1989] and *Rosengaus* [1987] during experiments using a movable sediment bed and similar wave conditions in the same wave flume. Information regarding the use of the experimental apparatus to obtain accurate measurements is presented in appropriate locations throughout this paper. More information on the experimental setup is given by *Mathisen and Madsen* [1996a], and detailed information on the setup is presented by *Mathisen and Madsen* [1993] and *Mathisen* [1993].

2.2. Roughness Determination

As noted previously, *Mathisen and Madsen* [1996a, b] used a modified form of the *Grant and Madsen* [1986] eddy viscosity model to analyze pure current, pure wave, and combined wave-current boundary layers. Modifications to this model included consideration of the phase difference between the bottom shear stress and near-bottom horizontal orbital velocity, consideration of an enhanced boundary layer thickness, and the effects of wave-induced mass transport. The model of *Madsen* [1994] also considers this phase difference, and the model can easily be modified to account for the enhanced boundary layer thickness and wave-induced mass transport. It also provides a consistent technique for comparing experimentally determined spectral wave roughnesses with the monochromatic wave roughnesses determined by the procedures of *Mathisen and Madsen* [1996a, b]. Therefore the *Madsen* [1994] model is selected for use in determining wave and current roughnesses in this study. As was the case for the application of the *Grant and Madsen* [1986] model by *Mathisen and Madsen* [1996a, b], the application of the *Madsen* [1994] model in the present analysis is considered to be formal since it involves an extrapolation of its range of validity to large roughness elements, which were necessary to generate rough turbulent boundary layers, and the choice of the *Madsen* [1994] model makes this model an integral part of the present study. Key aspects of the *Madsen* [1994] model that are relevant to this paper, as well as any required modifications to this model, are presented in appropriate locations in the text of this paper, and the reader is referred to *Madsen* [1994] for any additional background and details pertaining to this model.

Accordingly, roughness determinations for spectral waves (wave roughnesses) in the presence and absence of a current are determined from measurements of wave attenuation by applying the techniques presented for monochromatic waves by *Mathisen and Madsen* [1996a] and extended to spectral waves by *Madsen* [1994]. The spectral wave roughnesses are compared with wave roughnesses experienced by monochromatic waves propagating over the same fixed rippled bed. Following the nomenclature of *Mathisen and Madsen* [1996a], pure wave experiments (experiments with no current present) are designated with a lower case letter, and combined wave-current experiments are designated with an upper case letter. Furthermore, pure wave roughnesses are designated as k_w and wave roughnesses in the presence of a current are designated as k_{wc}. The values of k_{wc} are also used to predict time-averaged velocity profiles using the model of *Madsen* [1994] with modifications suggested by *Mathisen and Madsen* [1996b]. These predicted velocity profiles are then compared with measured time-averaged velocity profiles.

3. Generation of Spectral Waves

In order to investigate the bottom roughness and energy dissipation associated with boundary layers for spectral waves, an appropriate wave spectrum must be generated. The ideal approach would be to generate a full continuous spectrum. However, the procedures for determining the wave roughness for these experiments require accurate measurements that provide estimates of the wave attenuation due to bottom friction. For a continuous spectrum, nonlinear interactions between the infinite number of components would preclude accurate measurement of the wave attenuation for specific wave frequencies. Therefore, for this paper, an appropriate continuous wave spectrum is first defined and is subsequently used only as a guide for developing a discrete wave spectrum.

3.1. Definition of a Continuous Wave Spectrum

The amplitudes, frequencies, and phases for the spectral waves utilized in this investigation are defined to conceptually simulate a one-dimensional Joint North Sea Wave Project (JONSWAP) spectrum modified for finite depth. This spectrum, which was initially developed during JONSWAP by *Hasselmann et al*. [1973], is selected for simulation owing to its demonstrated success in providing an ideal representation of typical, real-world ocean wave spectra [e.g., *Hasselmann et al*., 1973; *Graber*, 1984]. The energy in a JONSWAP spectrum, E_J, is given by

$$E_J = E_{\mathrm{PM}} \gamma \exp\left[-(\omega/\omega_p - 1)^2/2\sigma^2\right] \tag{1}$$

where γ is a peak enhancement factor, ω_p is the radian frequency associated with the peak spectral energy, σ is a spectral width factor, and E_{PM} is the spectral energy for the Pierson-Moskowitz spectrum:

$$E_{\mathrm{PM}} = \frac{\alpha g^2}{\omega^5} \exp\left[-\frac{5}{4}\left(\frac{\omega_p}{\omega}\right)^4\right] \tag{2}$$

where α is Phillip's constant. As a spectrum enters finite depths, the shape of the spectrum typically gets skewed such

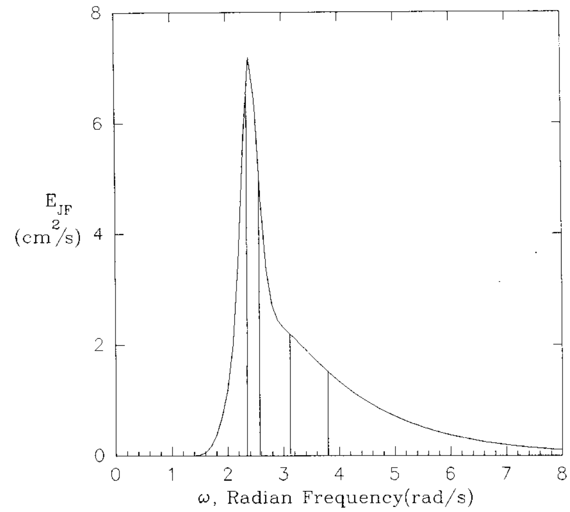

Figure 1. Spectral energy distribution for experiment s (with a design amplitude a_{rep} of 4 cm) showing energy partitions for five spectral components.

that energies are increased at the lower frequencies of the distribution. Following *Kitiagorodskii et al.* [1975], *Graber* [1984] defined a finite depth JONSWAP spectrum as

$$E_{JF} = \phi(\omega) E_J \tag{3}$$

where $\phi(\omega)$ is obtained from

$$\phi(\omega) = \chi^{-2}[1 + \omega_h^2(\chi^2 - 1)]^{-1} \tag{4}$$

with

$$\omega_h = \omega[h/g]^{1/2} \tag{5}$$

in which h is the still water depth, g is gravitational acceleration, and χ is obtained from

$$\chi \tanh(\omega_h^2 \chi) = 1 \tag{6}$$

An appropriate spectrum is determined by adjusting the spectral energy distribution to match the characteristics of a representative monochromatic wave (defined by amplitude a_{rep} and radian frequency ω_{rep}). The spectral energy distribution for experiment s (where the lower case letter designation indicates that no current is present) is shown by the solid line in Figure 1. This spectrum is developed by choosing values of 3.3 for γ and 0.08 for σ (which closely match typical values noted by *Graber* [1984]), setting ω_p equal to ω_{rep}, and adjusting α such that E_S matches the energy associated with the representative monochromatic wave, given by

$$E_S = \int_0^\infty E_{JF}(\omega)\, d\omega = \frac{1}{2} a_{\mathrm{rep}}^2 \tag{7}$$

Conditions for spectral experiments were developed based on a representative radian frequency of 2.18 rad/s and representative amplitudes of 4, 5, and 6.7 cm. The corresponding values of α for these experiments are 0.00056, 0.00084 and 0.00157, respectively.

3.2. Development of a Discrete Wave Spectrum

To reduce the complicating effects of wave-wave interactions in these experiments, the continuous wave spectrum described in the previous section is approximated by a discrete wave spectrum. A discrete spectrum can be generated in the wave flume by superimposing a finite number of wave components with different discrete frequencies and amplitudes chosen to approximate the spectral energy distribution of the continuous spectrum. Accordingly, for a spectrum of progressive waves with N components, the water surface profile η may be represented by

$$\eta = \sum_{j=1}^{N} \eta_j = \sum_{j=1}^{N} a_j \cos(k_j x - \omega_j t + \theta_j) \tag{8}$$

where, for the jth component, η_j is the surface profile variation, a_j is the amplitude, ω_j is the radian frequency, θ_j is a random phase angle, and k_j is the wave number defined by the dispersion relationship

$$\omega_j^2 = g k_j \tanh k_j h \tag{9}$$

In this case, the total spectral energy E_S can be written as

$$E_S = \sum_{j=1}^{N} \frac{1}{2} a_j^2 = \frac{1}{2} a_{\mathrm{rep}}^2 \tag{10}$$

where the total energy equals the sum of energies associated with individual wave components.

The ideal approach to approximate the continuous spectrum by a discrete spectrum is to define the frequencies and energies for the individual wave components such that the collective energy distribution closely matches the energy distribution of the continuous spectrum. To represent the characteristics of a continuous wave spectrum by an N component discrete spectrum, the area under the spectral energy distribution is integrated and the spectral energy distribution is partitioned into N portions, with each portion represented by a separate wave component with an amplitude, frequency, and phase.

For these experiments, spectral simulations were defined in terms of five wave components. Representation of the spectrum in terms of five components was found to ensure sufficiently large (and measurable) wave attenuation and to accommodate the physical requirements of wave generation using a wave maker as clarified in the following description of wave maker operation. It is noted that the complexity of a JONSWAP spectrum cannot be fully characterized by using five wave components. However, a five-component spectrum is considered to be adequate to verify the assumption of a single roughness and application of a monochromatic wave to represent a multicomponent spectrum, which are the objectives of this investigation.

For this case, the spectral energy dissipation can be represented using one of two approaches. First, a set of equally spaced frequency components could be defined and the wave amplitudes could be adjusted to model the energy distribution in the spectrum. Second, a set of equal wave component amplitudes could be determined (from (10)) and the frequencies could be adjusted to model total energy in the spectrum. Owing to the shape of the spectrum in Figure 1, most energy is contained within the near-peak frequency wave components. If the first approach is used, wave amplitudes for the lowest- and highest-frequency components will be too small for wave attenuation to be measured accurately. Therefore the second approach is selected for this paper and the portions of the spectrum are represented using equal wave component amplitudes with appropriately adjusted component frequencies. The energy partitions obtained using this approach for the five-component discrete spectrum for experiment s are shown as the vertical lines in Figure 1.

Frequencies for the individual components are defined as the centroids of the partitions in the spectral energy distribution. The frequencies are subsequently adjusted slightly to ensure that the actual component frequencies precisely equal the discrete frequencies resolved by the fast Fourier transform (FFT) algorithm used for the analysis of wave amplitude attenuation. In addition, as clarified in section 4, energy dissipation is a function of the near-bottom horizontal orbital velocity, which is given by

$$u_{bm,j} = \frac{a_j \omega_j}{\sinh k_j h} \tag{11}$$

To assure that wave attenuation can be measured with the same accuracy for each individual wave component, amplitudes are adjusted such that the near-bottom horizontal orbital bottom velocity is effectively the same for every component of the spectrum. Since the accuracy of each wave attenuation measurement is the same, this approach provides an ideal format for comparison with predictions of the *Madsen* [1994] model. Finally, the nature of (8) indicates that, at any given location along the length of the flume, the phase difference between any two of the five wave components varies in time, effectively simulating a random phase difference. The phase differences between individual wave components were also shown to be inconsequential in the movable bed experiments presented by *Madsen et al*. [1990]. Accordingly, a single set of random phases was selected for the five wave components, and this same set of phases was used for all three different spectral wave conditions simulated.

Once the amplitudes, frequencies, and phases for the wave components were defined, the discrete spectrum could be generated by superimposing the wave maker paddle motion for individual wave components, where the wave maker paddle motion for each component is determined following the linear theory of *Biésel and Suquet* [1951]. Precautions were taken to ensure that the water characteristics (e.g., temperature) and equipment operation were the same for all of the experiments completed. One hour of warm-up time was provided, and the water in the flume was thoroughly mixed. In accordance with the results of preliminary experiments, at least 20 min were provided after the initiation of wave maker motion before taking measurements to allow the wave spectrum to reach a fully developed state. To illustrate how the approach effectively simulates a random spectrum, a typical measured water surface variation record is shown in Figure 2 for experiment s. The measurement and subsequent use of this record are discussed further in section 4.

4. Determination of the Spectral Wave Attenuation Due to Bottom Friction

4.1. Determination of the Total Spectral Wave Attenuation

Total wave attenuation was determined from time records of water surface elevations, which were measured using conductivity-type wave gauges as detailed by *Mathisen and Madsen* [1996a]. Wave gauges were recalibrated before each experimental run, and wave gauge output was monitored before and

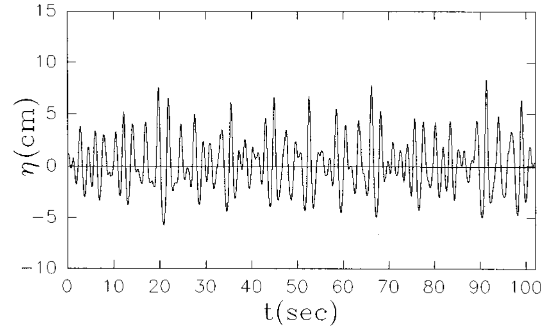

Figure 2. Water surface variation for experiment s, measured 5 m from wave maker.

after each run to ensure that any drift associated with electronics or water characteristics did not prevent accurate water level measurement. The surface profile variation is represented using a sampling duration of 102.4 s, which represents the periodicity of the five-component spectral simulation. Energy dissipation and, subsequently, the bottom roughness experienced by spectral waves were determined by analyzing measurements of wave attenuation. Accordingly, surface profile time records (similar to the record shown in Figure 2) were obtained for 20 locations along the length of the wave flume and used to determine wave attenuation for each experiment.

An FFT algorithm was used to convert the surface elevation time records into frequency records of amplitude and phase. Typical amplitude spectra for experiment s, measured 5 and 16.25 m downstream from the wave maker, are shown in Figure 3. Primary amplitudes for the five wave components dominate other components and are clearly defined. Amplitudes at 16.25 m are generally lower than those at 5 m, indicating, as expected, that some wave attenuation exists. It can also be noted that high-frequency residual components at 16.25 m tend to be lower than the corresponding high-frequency residual components at 5 m, whereas the reverse is true for the low-frequency residual components. These tendencies indicate the presence of nonlinear energy transfers in accordance with the theory of *Hasselmann* [1962].

Measured amplitudes for each primary frequency indicated

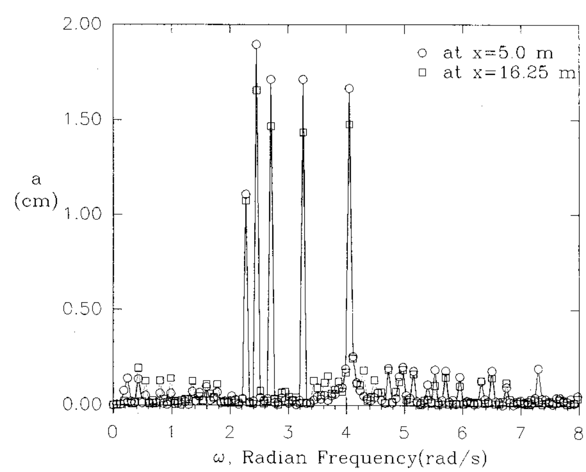

Figure 3. Experimentally-determined discrete wave amplitude spectrum for experiment s (actual a_{rep} = 3.65 cm), measured at 5 and 16.25 m from wave maker.

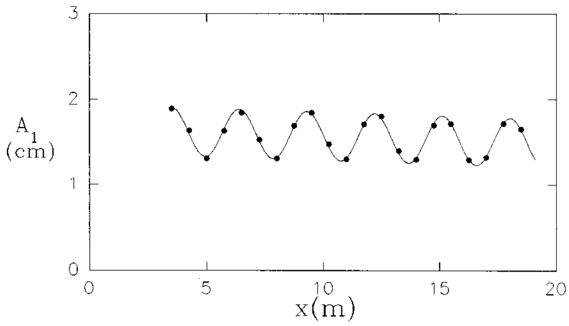

Figure 4. Wave amplitude variation along test section of flume for lowest-frequency wave component ($T = 2.768$ s) of experiment s.

in Figure 3 include the effects of both incident and reflected components. These components are resolved for each frequency by fitting a least squares curve to the spatial wave amplitude variation as presented by *Mathisen and Madsen* [1996a]. The total amplitude variation along the flume's test section for the jth component, A_j, is approximated by

$$A_j = a_{o,j} + m_{t,j}x + a_{r,j}\cos[(k_{i,j} + k_{r,j})x + (\varphi_{r,j} - \varphi_{i,j})] \quad (12)$$

where $a_{o,j}$, $k_{i,j}$, and $\varphi_{i,j}$ are the amplitude, wave number, and phase, respectively, of the jth component of the incident wave with $a_{o,j}$ evaluated at the wave maker ($x = 0$); $a_{r,j}$, $k_{r,j}$, and $\varphi_{r,j}$ are the amplitude, wave number, and phase, respectively, of the jth reflected wave component; and $m_{t,j}$ is the total amplitude attenuation slope. Since the beach of the flume is covered with filter material and reflected amplitudes are reduced to less than 20% of the incident amplitudes, attenuation of the reflected component is neglected in (12). For waves in the presence of a current with an average velocity U, $k_{i,j}$ is related to an absolute radian frequency ω_j using (9) with k_j replaced by $k_{i,j}$ and ω_j replaced by $\omega_{i,j}$, where $\omega_{i,j}$ is defined as $(\omega_j - k_{i,j}U)$, which represents the radian frequency relative to the current. The wave number for the reflected wave, $k_{r,j}$, is determined from (9) with k_j replaced by $k_{r,j}$ and ω_j replaced by the radian frequency relative to the current for the reflected wave, $\omega_{r,j}$ (defined as $\omega_j + k_{r,j}U$). For pure waves with no current, $k_{i,j}$ equals $k_{r,j}$ and a single wave number k_j is determined directly from (9). Since the wavelengths for all components are between 2.5 and 6.5 m, the length of the flume's test section is no more than six wavelengths for any wave component. Therefore $m_{t,j}$ is approximated by a linear change in amplitude per unit length along the flume.

The amplitude variation for the lowest-frequency component ($j = 1$) for experiment s is shown along with the corresponding least squares curve fit using (12) in Figure 4. With $a_{o,1} = 1.311$ cm, $a_{r,1} = 0.260$ cm, $(\varphi_{r,1} - \varphi_{i,1}) = 1.4$ rad, and $m_{t,1} = -0.00002853$ cm/cm, the curve fit afforded by (12) provides an excellent match with the measured data (since the root-mean-square error is within 0.02 cm). Since values for $a_{o,j}$ and $m_{t,j}$ are used further for analysis of wave attenuation, these values are included along with the summary of experimental data tabulated in Table 1. Definitions for other parameters listed in Table 1 are provided in the text throughout this paper as appropriate.

4.2. Isolation of the Bottom Friction Slope

The variation in incident wave amplitude indicated by $m_{t,j}$ can be attributed to energy dissipation due to sidewall and bottom friction and to nonlinear energy transfers between various frequency components in the flume. In terms of the total attenuation slope, this relationship may be written as

$$m_{t,j} = m_{b,j} + m_{sw,j} + m_{nl,j} \quad (13)$$

where $m_{b,j}$ is the bottom friction slope, $m_{sw,j}$ is a sidewall dissipation slope, and $m_{nl,j}$ is an amplitude slope associated with nonlinear energy transfers. For the purposes of discussion, an amplitude change δa over the flume test section may be defined for a particular wave component as the total amplitude slope multiplied by 17 m (the length of the flume test section). Figure 5a shows the values for δa for each of the five components in the flume for experiment s. Frequencies, horizontal near-bottom orbital velocities, and other pertinent information corresponding to the five components can be found in Table 1. Amplitude changes are generally negative, indicating an expected decrease in energy along the length of the flume owing to bottom and sidewall friction. Since the $u_{b,j}$ values for all wave components are effectively the same, the dissipation changes for the various components would be expected to be the same as well. However, the total amplitude changes are larger for the higher-frequency components, with the lowest-frequency component effectively experiencing a negligible amplitude change. These trends are a result of nonlinear energy transfers that exist between various wave components in the flume. To isolate the amplitude changes due to bottom friction, it is necessary to remove the effects of these nonlinear energy transfers as well as any effects of sidewall dissipation.

These two effects may be estimated by completing experiments using a flat bed with no ripples in place. Flat bed experiments were conducted using the same experimental conditions as those with a rippled bed. The attenuation results for the flat bed experiments (including the estimated amplitude at the wave maker, $a_{ofb,j}$, and the flat bed total attenuation slope, $m_{tfb,j}$) are also included in Table 1. The wave period for the smooth and rippled bed tests is exactly the same since the wave maker operation is exactly the same for the two cases. In addition, as is evident in Table 1, the amplitudes for individual wave components are equivalent for the flat and rippled bed experiments. To illustrate the relationship between flat bed attenuation and rippled bed attenuation, total amplitude changes for the flat bed experiments are shown for experiment s in Figure 5b. For this case, the amplitude change is positive for the lowest-frequency component, negligible for the second-lowest-frequency component, and negative for the three highest-frequency components. This trend indicates that energy for this experiment is generally transferred from higher- to lower-frequency components, in agreement with expectations for nonlinear wave-wave interactions [*Hasselmann*, 1962]. Detailed evaluation of these wave-wave interactions is not pursued further here, since analysis of the nonlinear energy transfer among frequency components is beyond the scope of the present study. However, the estimates of the nonlinear energy transfers in flat bed experiments provide the basis for isolating the wave attenuation due to bottom friction in rippled bed experiments.

Since the experimental conditions are effectively the same for the flat bed experiments and rippled bed experiments, the nonlinear energy transfers and sidewall dissipation should be

Table 1. Attenuation Results for Combined Spectral Wave-Current Flow Experiments

Component Number j	U, cm/s	T_j, s	$a_{o,j}$, cm	$m_{t,j}$, cm/cm	$u_{bm,j}$, cm/s	$a_{ofb,j}$, cm	$m_{tfb,j}$, cm/cm	$m_{b,j}$, cm/cm	$f_{e,j}$	$f_{wc,j}$	u_{*wm}, cm/s	u_{*c}, cm/s	z_{oa}, cm	k_{wc}, cm
Experiment s														
1	···	2.768	1.311	−.0000285	4.64	1.237	.0000626	−.0000956	0.419	0.458				
2	···	2.560	1.657	−.0000891	5.55	1.633	−.0000025	−.0000923	0.335	0.481				
3	···	2.276	1.639	−.0001420	5.14	1.603	−.0000474	−.0001002	0.392	0.518				
4	···	1.933	1.715	−.0001448	4.96	1.673	−.0000526	−.0000982	0.387	0.575				
5	···	1.553	1.796	−.0001904	4.30	1.686	−.0000524	−.0001438	0.646	0.663				
Rep	···	2.171	3.65		11.03				0.420	0.533	5.69	···	···	27.6
Experiment t														
1	···	2.768	1.530	.0000184	5.60	1.573	.0000783	−.0000656	0.201	0.309				
2	···	2.560	1.915	−.0000695	6.54	1.946	.0000592	−.0001358	0.355	0.324				
3	···	2.276	1.918	−.0001752	5.98	1.996	−.0000964	−.0000857	0.243	0.347				
4	···	1.933	2.108	−.0002433	5.89	2.110	−.0001041	−.0001466	0.413	0.384				
5	···	1.553	2.024	−.0001851	4.92	2.155	−.0001425	−.0000498	0.164	0.440				
Rep	···	2.184	4.27		12.99				0.287	0.357	5.49	···	···	17.1
Experiment u														
1	···	2.768	2.126	.0000548	7.88	2.109	.0002233	−.0001765	0.290	0.231				
2	···	2.560	2.571	−.0000882	8.79	2.584	.0001227	−.0002043	0.322	0.241				
3	···	2.276	2.616	−.0003119	7.92	2.640	−.0002007	−.0002007	0.194	0.258				
4	···	1.933	2.764	−.0003591	7.60	3.050	−.0003559	−.0000132	0.020	0.284				
5	···	1.553	2.689	−.0003600	6.24	2.775	−.0002625	−.0001065	0.209	0.324				
Rep	···	2.213	5.73		17.29				0.215	0.263	6.27	···	···	13.8
Experiment S														
1	···	2.768	1.260	−.0000268	4.52	1.217	.0000445	−.0000752	0.386	0.379				
2	···	2.560	1.418	−.0000350	4.99	1.396	.0000321	−.0000717	0.332	0.397				
3	···	2.276	1.428	−.0000754	4.75	1.408	−.0000114	−.0000687	0.333	0.426				
4	···	1.933	1.601	−.0001084	4.89	1.601	−.0000395	−.0000742	0.344	0.469				
5	···	1.553	1.664	−.0001682	4.28	1.648	−.0000789	−.0000945	0.497	0.536				
Rep	16	2.152	3.31		10.49				0.370	0.459	5.02	2.71	1.76	17.5
Experiment T														
1	···	2.768	1.536	−.0000079	5.59	1.506	.0000779	−.0000910	0.300	0.330				
2	···	2.560	1.765	−.0000186	6.27	1.787	.0000741	−.0000988	0.288	0.346				
3	···	2.276	1.798	−.0001200	5.87	1.796	−.0000292	−.0000968	0.302	0.370				
4	···	1.933	2.050	−.0001950	6.03	1.992	−.0000134	−.0001885	0.561	0.408				
5	···	1.553	2.035	−.0002270	5.10	2.095	−.0002162	−.0000170	0.061	0.466				
Rep	12	2.174	4.13		12.94				0.317	0.393	5.74	2.35	2.77	18.0

Here "rep" refers to the characteristics associated with the representative wave.

effectively the same for both sets of experiments. Any differences between amplitude changes in flat bed and rippled bed experiments should then be a result of differences in amplitude attenuation in the bottom boundary layer. For the flat bed experiments, Reynolds numbers are of the order of 1200 to 1500, which indicates that boundary layers are laminar for flat bed experiments. Although energy dissipation in each laminar boundary layer is generally less than 10 to 15% of the energy dissipation in the turbulent boundary layer, laminar wave attenuation is estimated and removed from the flat bed attenuation results for completeness. *Hunt* [1952] estimated wave attenuation due to energy dissipation in laminar boundary layers for monochromatic waves. By extending this analysis to spectral waves, a wave attenuation slope for the jth component due to energy dissipation in a laminar boundary layer over the flat bed, $m_{fblam,j}$, can be approximated as

$$m_{fblam,j} = -\frac{1}{2}\sqrt{\frac{\nu}{2\omega_j}}\,\frac{\omega_j u_{bm,j}^2}{g c_{g,j} a_{m,j}} \tag{14}$$

where ν is the kinematic viscosity. For the flat bed experiments, (13) also applies, although, for clarity, $m_{t,j}$ can be denoted as $m_{tfb,j}$ and $m_{b,j}$ can be denoted as $m_{fblam,j}$, since the laminar attenuation given by (14) is appropriate. Using the notation "*rb*" to indicate measurements with a rippled bed in place and the notation "*fb*" to indicate measurements with a flat bed with experimental conditions similar to those for the rippled bed, amplitude slopes associated with nonlinear energy transfers and sidewall dissipation for the jth component of the rippled bed experiments, $[m_{nl,j} + m_{sw,j}]_{rb}$, can be approximated by $[m_{nl,j} + m_{sw,j}]_{fb}$. Then, $[m_{nl,j} + m_{sw,j}]_{fb}$ is equal to $[m_{tfb,j} - m_{blam,j}]_{fb}$, where $m_{blam,j}$ is given by (14) and an expression for the bottom friction slope of the jth component for a rippled bed experiment is obtained by modifying (13) to read

$$m_{b,j} = m_{t,j} - [m_{sw,j} + m_{nl,j}]_{rb} = m_{t,j} - [m_{tfb,j} - m_{blam,j}]_{fb} \tag{15}$$

These procedures also apply for waves in the presence of a current, in which (14) is modified by replacing $c_{g,j}$ by $(c_{g,j} + U)$ and ω_j by $\omega_{i,j}$.

Wave attenuation slopes determined in this manner can also be interpreted in terms of an amplitude change that is strictly associated with bottom friction. Amplitude changes strictly due to bottom friction are estimated by subtracting the flat bed amplitude changes shown in Figure 5b (after removing the effects of laminar bottom friction) from the total amplitude changes (shown in Figure 5a). The resulting amplitude changes due to bottom friction are shown in Figure 5c. All amplitude

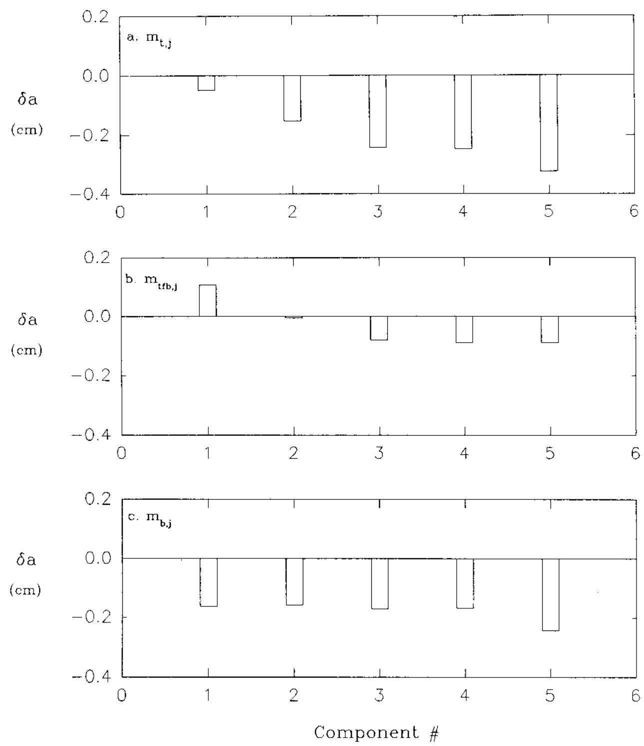

Figure 5. Amplitude changes for five wave components of experiment s. (a) Total amplitude changes measured over a rippled bed. (b) Total amplitude changes measured over a flat bed. (c) Amplitude changes resulting strictly from bottom friction.

changes are now negative, indicating a decrease in energy due to bottom friction. Amplitude changes are also similar for all components, with the exception of the highest-frequency component, which is slightly higher than the others.

4.3. Review of Attenuation Results

The total attenuation slopes ($m_{t,j}$), flat bed attenuation slopes ($m_{tfb,j}$), and bottom friction slopes ($m_{b,j}$) for all experiments can be found in Table 1. For experiment s (which was for pure waves) and experiment S (which included a current), the bottom friction slopes are similar for the five spectral wave components. The $m_{b,j}$ estimates are also similar for the five frequencies of experiments t, T, and u. For these three experiments, however, some variability is apparent in the $m_{b,j}$ estimates, and this variability appears to increase with spectral energy. Since repeated experiments indicated that the amplitudes could be measured within 0.02 cm, this variability is not considered to be associated with random experimental error. Rather, it is likely that the apparent variability for higher spectral intensities results from differences between the properties of wave components in the flat bed and rippled bed experiments, which are more pronounced for higher spectral energies.

Comparisons of near-bottom horizontal orbital velocities for the flat bed and rippled bed experiments can be used to demonstrate the significance of these differences. Since differences in bottom friction between flat and rippled bed conditions result in slightly different values of $u_{bm,j}$ at the flume midpoint, $u_{bm,j}$ was recalculated using the wave amplitude located adjacent to the wave maker to avoid these differences. These values were then used to calculate values for $u_{bm,j}/u_{bm,1}$ (in which $u_{bm,1}$ is arbitrarily selected as a component for comparison), and the results are summarized in Table 2. First, comparison of the values of $u_{bm,j}/u_{bm,1}$ for each selected frequency of the rippled bed runs of experiments s, t, and u (the three pure wave experiments) reveals that the values of the parameter are similar for all three experiments and decrease slightly with increasing spectral intensity. Values of this parameter are also effectively the same for each selected frequency for experiments S and T (the two wave-current experiments). These results indicate that the wave spectra are repeatable and similar in nature for all rippled bed experiments.

Next, review of the values of $u_{bm,j}/u_{bm,1}$ for each selected frequency of the flat bed experiments listed in Table 2 indicates that the trends of the spectral distributions for the flat bed experiments are similar to those of the rippled bed experiments. However, direct comparisons between $u_{bm,j}/u_{bm,1}$ values for similar components of flat bed and rippled bed runs do indicate some slight differences. The interactions differ for rippled and flat bed experiments because differences in wave attenuation lead to slightly different amplitudes and phase relationships among the various wave components for the two cases. Since the extrapolation of the curve fits obtained from amplitude data measured in the flume's test section would tend to exaggerate any experimental error, the differences apparent in Table 2 are likely conservative estimates. However, the corresponding differences between $u_{bm,j}/u_{bm,1}$ values for rippled and flat bed experiments are all less than 0.07, with the only exceptions being the fourth frequency component (T = 1.933 s) for experiment u and the highest-frequency components (T = 1.533 s) for experiments S and T. Review of $m_{b,j}$ determinations reveals that the associated $m_{b,j}$ values for these specific cases are also different from the other estimates. Since this variability is well within our present ability to predict energy dissipation for spectral wave components, the $m_{b,j}$ values listed in Table 1 are accepted as adequate indicators of

Table 2. Ratio of Near-Bottom Horizontal Orbital Velocity for Individual Wave Components ($u_{bm,j}$) to the Near-Bottom Horizontal Orbital Velocity for the Lowest-Frequency Component ($u_{bm,1}$): Comparisons Between Flat and Rippled Bed Experiments

		Experiment s		Experiment t		Experiment u		Experiment S		Experiment T	
Component Number j	T_j, s	Rippled	Flat	Rippled	Flat	Rippled	Flat	Rippled	Flat	Rippled	Flat
1	2.768	1.00	1.00	1.00	1.00	1.00	1.00	1.00	1.00	1.00	1.00
2	2.560	1.24	1.29	1.23	1.21	1.19	1.20	1.11	1.12	1.13	1.16
3	2.276	1.18	1.22	1.18	1.25	1.16	1.17	1.08	1.10	1.11	1.13
4	1.933	1.15	1.18	1.20	1.17	1.14	1.26	1.14	1.17	1.18	1.18
5	1.533	1.02	1.01	0.98	1.01	0.93	0.97	1.13	0.98	0.98	1.07

wave attenuation due to energy dissipation in the bottom boundary layer. The overall uniformity in amplitude changes (and hence $m_{b,j}$ estimates) for all frequency components (as is apparent in Figure 5c), a result of the selection of wave components with equal near-bottom horizontal orbital velocities (as can be seen in Table 1), provides an adequate basis for analysis of energy dissipation to determine the bottom roughness for spectral waves.

5. Bottom Roughness for Waves in the Presence and Absence of a Current

5.1. Energy Dissipation

Energy dissipation for pure spectral wave boundary layers was modeled by *Madsen et al.* [1988]. This analysis was generalized for combined spectral wave-current flows by *Madsen* [1994]. *Madsen* [1994] represented the near-bottom characteristics of a wave spectrum in terms of a representative near-bottom horizontal bottom velocity, $u_{bm,r}$, defined by

$$u_{bm,r} = \sqrt{\sum_{j=1}^{N} u_{bm,j}{}^2} \tag{16}$$

and a radian frequency ω_r,

$$\omega_r = \frac{\sum_{j=1}^{N} \omega_{i,j} u_{bm,j}{}^2}{\sum_{j=1}^{N} u_{bm,j}{}^2} \tag{17}$$

where $u_{bm,j}$ and $\omega_{i,j}$ are the maximum near-bottom horizontal orbital velocity and radian frequency of the jth component, respectively. These values are listed as the representative values in Table 1, where the representative period $T_{\text{rep}} = 2\pi/\omega_r$.

Following the approach of *Kajiura* [1968], *Madsen* [1994] estimated the rate of energy dissipation in the bottom boundary layer for each wave component as

$$E_{d,j} = \overline{\tau_{b,j}(t) u_{b,j}(t)} = \frac{1}{4} \rho \sqrt{f_{wc,r}} \sqrt{f_{wc,j}} \cos \varphi_j u_{bm,r} u_{bm,j}^2 \tag{18}$$

where ρ is the fluid density; $f_{wc,r}$ is a representative wave friction factor; $u_{bm,r}$ is the representative horizontal near-bottom orbital velocity given by (16); and, for the jth component, $\tau_{b,j}(t)$ is bottom shear stress; $u_{b,j}(t)$ is the horizontal near-bottom orbital velocity; $f_{wc,j}$ is a friction factor; $u_{bm,j}$ is the near-bottom horizontal orbital velocity; and φ_j is the phase angle between the bottom shear stress and near-bottom horizontal orbital velocity. Owing to the significant effect the value of $u_{bm,j}$ has on the energy dissipation given by (18), selection of wave components with equal near-bottom horizontal orbital velocities leads to approximately equal amounts of energy dissipation for different frequency components.

Energy dissipation can also be conveniently characterized in terms of an energy dissipation factor. By defining an energy dissipation factor $f_{e,j}$, such that

$$f_{e,j} = \sqrt{f_{wc,r}} \sqrt{f_{wc,j}} \cos \varphi_j \tag{19}$$

(18) can be incorporated into the conservation of wave energy equation

$$\frac{\partial}{\partial x}\left[\frac{1}{2}\rho g a_j^2 (c_{g,j} + U)\right] = \rho g a_{m,j} m_{b,j} (c_{g,j} + U)$$
$$= -\frac{1}{4} \rho f_{e,j} u_{bm,r} u_{bm,j}^2 \tag{20}$$

which simply represents an extension of the procedure presented by *Mathisen and Madsen* [1996a] to the jth wave component of a wave spectrum. In (20), $a_{m,j}$, $c_{g,j}$, and $u_{bm,j}$ are the mean amplitude, group velocity (taken relative to the current), and near-bottom horizontal orbital velocity for the jth component, respectively. The mean amplitude $a_{m,j}$ represents the incident amplitude evaluated from the first two terms in (12) at the midpoint of the test section (i.e., at $x = 10$ m from the wave maker). Values for the near-bottom horizontal orbital velocity $u_{bm,j}$ are determined from (11) with a_j replaced by $a_{m,j}$, ω_j replaced by $\omega_{i,j}$, and k_j replaced by $k_{i,j}$. These values can then be used in conjunction with (16) to calculate $u_{bm,r}$. Calculated values for $f_{e,j}$, determined from experimental data using (20), are listed along with values for $m_{b,j}$, $u_{bm,j}$ and $u_{bm,r}$ in Table 1. From (20), it follows that a representative energy dissipation factor is defined by

$$f_{e,r} = \frac{\sum_{j=1}^{N} f_{e,j} u_{bm,j}{}^2}{\sum_{j=1}^{N} u_{bm,j}{}^2} \tag{21}$$

Values of $f_{e,r}$ for the individual experiments are listed in Table 1.

5.2. Bottom Roughness for Spectral Waves

Following *Grant and Madsen* [1986], *Mathisen and Madsen* [1996a] presented a methodology to relate the energy dissipation factor for monochromatic waves to a bottom roughness, k_{wc}, by evaluating the shear stress at the elevation of the hydraulic roughness, $z = z_o$. *Madsen* [1994] used the equivalent wave concept to extend this methodology to relate k_{wc} to $f_{wc,r}$ for spectral wave-current boundary layer flows and developed explicit relationships for the wave friction factor and phase angle for the representative wave defined by (16) and (17). First, a maximum combined shear velocity u_{*r} is defined, which, for codirectional waves and currents, is given by

$$u_{*r}{}^2 = u_{*c}{}^2 + u_{*wm,r}{}^2 \tag{22}$$

where u_{*c} is the current shear velocity and $u_{*wm,r}$ is the maximum wave shear velocity of the representative wave. Next, a coefficient C_μ is defined as $(1 + \mu)$ with μ given by $(u_{*c}/u_{*wm,r})^2$, where $u_{*wm,r}$ is related to the wave friction factor $f_{wc,r}$ through

$$\frac{\tau_{bw,r}}{\rho} = u_*{}^2_{wm,r} = \frac{1}{2} f_{wc,r} u_{b,r}^2 \tag{23}$$

following *Jonsson* [1966]. For the range $0.2 < C_\mu u_{bm,r}/(k_{wc}\omega_r) < 10^2$, which is appropriate for the experiments presented in this paper, the $f_{wc,r}$ to k_{wc} relationship (presented as equation (32) of *Madsen* [1994]) is given by

$$f_{wc,r} = C_\mu \exp\left[7.02\left(\frac{C_\mu u_{bm,r}}{k_{wc}\omega_r}\right)^{-0.078} - 8.82\right] \tag{24}$$

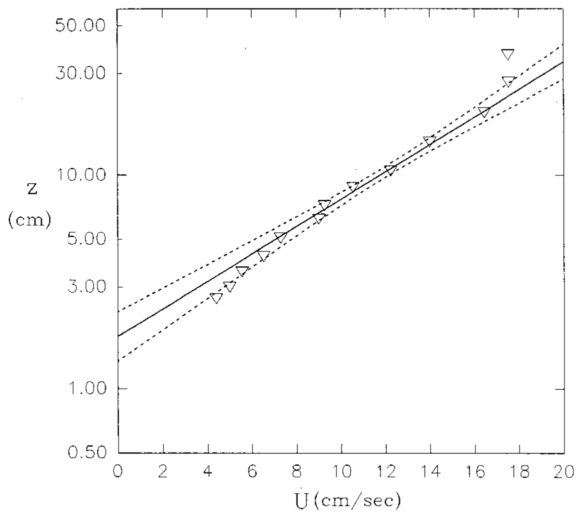

Figure 6. Time-averaged velocity profile for experiment S, current shear velocity u_{*c} determination.

and the phase angle in degrees (presented as equation (39) of *Madsen* [1994]) is approximated by

$$\varphi_r = 33 - 6.0 \log \frac{C_\mu u_{bm,r}}{k_{wc}\omega_r} \tag{25}$$

For waves in the presence of a current, $u_{*wm,r}$ (and therefore C_μ) is not known a priori, and an iterative technique is necessary to determine k_{wc}. The iterative technique for the present case requires values for the current shear velocity u_{*c} as input. Estimates for u_{*c} are determined by fitting time-averaged current velocity profiles in the presence of waves with a logarithmic expression of the form

$$u = \frac{u_{*c}}{\kappa} \ln \frac{z}{z_{oa}} \tag{26}$$

where κ is von Karman's constant (taken to be 0.4) and z_{oa} is an apparent hydraulic roughness. The current velocity profile for experiment S, measured over the crest with the reference elevation ($z = 0$) set at the flume bottom, is shown in Figure 6. In this profile, a clearly delineated logarithmic region is observed between 6 and 15 cm. The region above 15 cm is in the free stream and is outside of the logarithmic region. The region below this logarithmic region is within the wave boundary layer. The best fit to the data within the logarithmic region is indicated by the solid line in Figure 6. This curve fit yields a current shear velocity of 2.71 cm/s and a measured apparent hydraulic roughness of 1.76 cm. The current shear velocities and measured apparent hydraulic roughnesses for both wave-current experiments are obtained in this manner and are included in Table 1.

With a value for the current shear velocity, the iterative procedure for determining k_{wc} can be initiated by assuming that C_μ equals 1 and φ_r equals 33°. Then, the energy dissipation factor, $f_{e,r}$, determined from (21) can be related to the representative wave friction factor for the equivalent monochromatic wave, $f_{wc,r}$, by applying (19) with $f_{e,j}$ replaced by $f_{e,r}$, $f_{wc,j}$ replaced by $f_{wc,r}$, and φ_j replaced by φ_r. Using the values of $f_{wc,r}$ and C_μ, k_{wc} can be estimated from (24). Also, (23) can be used to determine $u_{*wm,r}$, from which a new value of C_μ can be determined. The new value of C_μ and the estimate for k_{wc} are then used to estimate a new value of φ_r. Using the values of C_μ and φ_r, the procedure is repeated until the values for k_{wc} converge. Note that for spectral waves with no current present, C_μ is equal to 1 and (24) and (25) can be used directly to determine $k_{wc} = k_w$.

Spectral wave roughness results and corresponding representative wave friction factors determined using this approach are listed in Table 1. Some variability is evident in the spectral wave roughness data, and trends in the wave roughness data appear to be related to the representative horizontal near-bottom excursion amplitude $A_{b,r}$. These trends are consistent with trends observed in monochromatic wave roughness results presented by *Mathisen and Madsen* [1996a]. However, as was the case in the work by *Mathisen and Madsen* [1996a], these trends are considered insufficiently persistent to be accounted for with the available data. Therefore mean values are used to compare spectral wave roughnesses with monochromatic wave roughnesses.

Mathisen and Madsen [1996a, b] presented results for the average bottom roughness experienced by monochromatic waves. In the preparation of the present paper, an unfortunate error was uncovered in the program used to calculate f_{wc} by *Mathisen and Madsen* [1996a, b]. This error had only minor effects on their calculated roughnesses, and the conclusions of these papers remain the same. For completeness, however, this error is discussed in the appendix, and corrected roughness values for monochromatic waves are presented in Table A1. Following *Mathisen and Madsen* [1996a] for the monochomatic wave experiments with 10-cm spacing, the arithmetic mean for the corrected k_w and k_{wc} values is now 18.6 cm, with a standard deviation of 4.3 cm. Since the arithmetic mean value for the roughnesses listed in Table 1 for the spectral wave experiments is 18.8 cm with a standard deviation of 5.2 cm, it is concluded that the average monochromatic and spectral roughnesses are equivalent within the accuracies indicated by the standard deviations. Since the bottom roughness enters (26) as an argument of the logarithm, *Mathisen and Madsen* [1996b] also used a geometric mean to compare roughness estimates. For this case, the geometric mean for the spectral wave roughness is 18.2 cm with a standard deviation of 4.8 cm, which closely matches the geometric mean of 18.1 for the monochromatic wave experiments. Whether the geometric or arithmetic mean roughness is considered, the excellent correspondence between the mean spectral wave roughness and mean monochromatic wave roughness indicates an agreement that is significantly better than our present ability to predict the bottom roughness for a movable sediment bed. Therefore, for practical purposes, the monochromatic and spectral roughnesses are considered to be the same.

6. Prediction of Spectral Wave Attenuation

If the bottom roughness is known or can be estimated, a spectral energy dissipation model may be used to provide predictions of spectral wave attenuation. A single energy dissipation factor $f_{e,r}$ is often used to characterize energy dissipation due to bottom friction for all components of the spectrum. The validity of this assumption can be investigated by using experimentally determined $f_{e,r}$ values for particular experiments to predict wave attenuation for individual wave components. In this case, bottom friction slopes are determined using (20) by replacing $f_{e,j}$ by $f_{e,r}$.

These bottom friction slopes are then used to predict am-

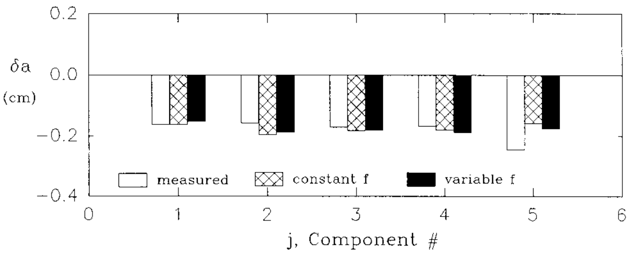

Figure 7. Comparisons between experimentally determined bottom friction amplitude changes and predicted amplitude changes for experiment s. Cross-hatched bars represent predictions using a constant friction factor, and solid bars represent predictions using model of *Madsen* [1994].

plitude changes for each component over the 17-m length of the flume. The predictions for experiment s are compared with measured attenuation data in Figure 7. Predicted amplitude changes represented by the cross-hatched bars closely match the measured amplitude changes represented by the unshaded bars. However, the predicted amplitude changes, obtained for a constant $f_{e,j} = f_{e,r}$, decrease slightly as frequency increases, while the measured amplitude changes increase slightly as frequency increases.

Wave attenuation for individual wave components can also be predicted using the theory of *Madsen* [1994], in which case final values for $f_{wc,j}$ are variable, since they are determined independently for each component. Following *Madsen* [1994], (24) and (25) can be rewritten to calculate the wave friction factor and the phase angle for individual wave components, $f_{wc,j}$ and φ_j. In this case, k_w or k_{wc} (already determined from (24) as discussed in the previous section) is used as input, and (24) is rewritten now as

$$f_{wc,j} = C_\mu \exp\left[7.02\left(\frac{C_\mu u_{bm,r}}{k_{wc}\omega_j}\right)^{-0.078} - 8.82\right] \quad (27)$$

and (25) is rewritten as

$$\varphi_j = 33 - 6.0 \log \frac{C_\mu u_{bm,r}}{k_{wc}\omega_j} \quad (28)$$

where both equations are applicable for the range $0.2 < C_\mu u_{bm,r}/(k_{wc}\omega_r) < 10^2$. The values for $f_{wc,j}$ and φ_j can then be used in conjunction with (19) and (20) to predict wave attenuation.

Again, bottom friction slopes ($m_{b,j}$) obtained from (20) can be interpreted in terms of an amplitude change across the length of the test section of the flume. Values for $f_{wc,j}$ and φ_j used in this calculation are obtained in this manner, and the resulting predictions for experiment s are compared with measured attenuation data in Figure 7. The predicted amplitude changes (shown by the solid bars) are similar in magnitude to the predicted amplitude changes assuming a constant $f_{e,j} = f_{e,r}$ (indicated by the crosshatched bars) and also agree well with the measured amplitude changes (represented by the unshaded bars). However, the predicted amplitude changes based on the *Madsen* [1994] theory provide a slightly improved correspondence with the trends of the measured amplitude changes for higher frequencies.

To compare the two approaches (i.e., use of a constant $f_{wc,j} = f_{wc,r}$ and use of a variable $f_{wc,j}$ as determined using the approach of *Madsen* [1994]), estimates for rms error were calculated for each experiment. The average rms errors for both approaches were 0.062 cm, indicating that the overall correspondence with measured data was the same for both approaches. Since the average wave attenuation due to bottom friction for individual wave components is approximately 0.18 cm, these results indicate that this error is less than 35% of the average wave attenuation. However, experiments s and S included lower wave intensities and show less variability than experiments t, T, and u. For experiment s, the use of a variable $f_{wc,j}$ yields an rms error of 0.036 cm (or approximately 20% of the attenuation), while the use of a constant $f_{wc,j}$ yields a slightly higher rms error of 0.043 cm (or approximately 24% of the attenuation). For experiment S (which included a current), the average attenuation for individual components is 0.13 cm, and, in this case, the rms error for a variable $f_{wc,j}$ is 0.017 cm (or approximately 13% of the attenuation) while the rms error for a constant $f_{wc,j}$ is 0.021 cm (or approximately 16% of the attenuation).

These comparisons show that the constant $f_{wc,j} = f_{wc,r}$ and variable $f_{wc,j}$ approaches both provide adequate matches to these data. This result can be explained by closer inspection of the nature of (27), where $f_{wc,j}$ is seen to be weakly dependent on $u_{bm,r}$ and ω_j, with no direct dependence on $u_{bm,j}$. Consequently, even if we subdivide the spectrum, $f_{wc,j}$ will not vary significantly. Moreover, since an increase in ω_j results in a slight increase in $f_{wc,j}$ and a slight increase in φ_j, the counteracting effects result in negligible change in $f_{e,j}$ when it is calculated from (19). Since the *Madsen* [1994] model provides a theoretical basis for a variable $f_{wc,j}$ and since the use of that model provides predictions that match the trends and magnitudes of the data, the *Madsen* [1994] model is recommended for prediction of wave attenuation. For higher wave conditions, additional research is still recommended to clarify which of these approaches is appropriate.

7. Wave-Current Interaction

Using wave roughnesses determined from wave attenuation measurements and current shear velocities determined from measured velocity profiles, the *Madsen* [1994] model can be used to predict velocity profiles for a current in the presence of waves. These predicted velocity profiles can be compared to measured velocity profiles to show that a single roughness and an equivalent monochromatic wave defined by (16) and (17) characterize combined spectral wave-current flows. The velocity profile for experiment S, predicted using a direct application of the *Madsen* [1994] model with a bottom roughness k_{wc} obtained from Table 1, is shown by the dotted line in Figure 8. As can be seen in Figure 8, the velocity profile obtained from a direct application of the *Madsen* [1994] model does not match the measured velocity profile. The same discrepancy was evident for experiment T.

However, the monochromatic experiments of *Mathisen and Madsen* [1996b] showed that velocity profiles for currents in the presence of monochromatic waves were affected by wave-induced mass transport and an enhanced wave boundary layer thickness resulting from the large roughness elements that were necessary to generate rough turbulent boundary layers in the flume. Review of Figure 8 reveals that velocity measurements follow a steeper velocity gradient for elevations lower than 6 to 7 cm. This region is indicative of a wave boundary layer region. This enhanced boundary layer thickness is similar to boundary layer thicknesses observed by *Mathisen and Mad-*

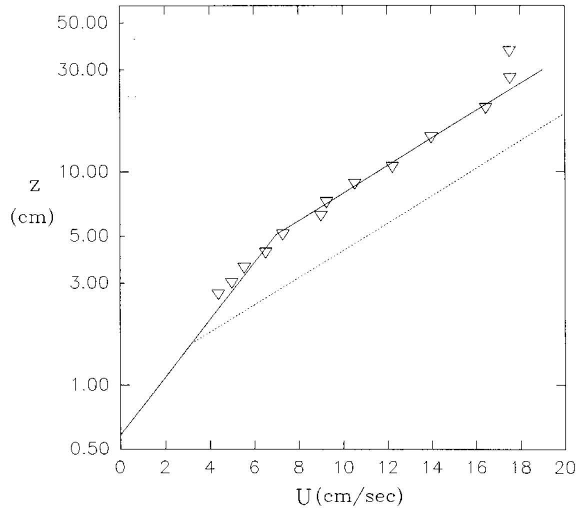

Figure 8. Time-averaged velocity profile for experiment S, comparisons with predictions of *Madsen* [1994] model (dotted line) and *Madsen* [1994] model incorporating the improved prediction of *Madsen and Salles* [1999] (solid line).

sen [1996b] for monochromatic waves over identical bottom roughness conditions.

Further evidence of the enhanced wave boundary layer thickness is provided by near-bottom wave velocity profiles measured in the flume 9.5 m downstream of the current inlet, which provided profiles of wave velocity amplitude and phase. Since velocity profiles were measured over a ripple crest, the wave velocity amplitudes near the bottom were distorted owing to the proximity of the ripple crest and therefore could not be used to accurately estimate the wave boundary layer thickness. Wave velocity phases, however, were not distorted extensively by the proximity of the ripple crest and could be used to estimate the wave boundary layer thickness. Profiles of the wave velocity phase, which are measured relative to the phase at 36 cm above the bottom, are shown in Figure 9 for all five components of the simulated wave spectrum. The phases generally reach a minimum at the 6-cm elevation and increase for lower elevations. If the boundary layer thickness is designated as the height in the measured profile at which the wave velocity phase reaches its lowest value, the boundary layer thickness shows a slight decrease with increasing frequency as expected. These trends are similar to the trends exhibited by the monochromatic wave profiles of *Mathisen and Madsen* [1996b] and led to the introduction of an enhanced wave boundary layer thickness δ_{wc}, which was set to be 6 cm.

The reason for *Mathisen and Madsen*'s [1996b] necessity to introduce the enhanced boundary layer thickness has been resolved analytically by *Madsen and Salles* [1999]. Madsen and Salles wrote the wave boundary layer thickness in the form

$$\delta_{wc} = A\,\frac{\kappa u_{*,m}}{\omega_r} \tag{29}$$

and defined this boundary layer thickness to be the height at which the wave velocity amplitude within the boundary layer is within 5% of the free stream velocity amplitude. *Grant and Madsen* [1986] estimated the coefficient A to be between 1 and 2. With the new approach of *Madsen and Salles* [1999], the value of A is found to depend on the value of A_b/k_n and increases as the value of A_b/k_n decreases. While the coefficient A is between 1 and 2 for A_b/k_n values between 100 and 1000, its value is significantly higher for the low A_b/k_n values associated with these experiments. The values of A for the two wave-current experiments were estimated from Table 1 of *Madsen and Salles* [1999]. For experiment S, with an A_b/k_n of 0.205, the value of A is estimated to be 6.5, in which case (29) yields a corresponding boundary layer thickness of 5.1 cm. When this modified boundary layer thickness is considered, the predicted velocity profile shown by the solid line in Figure 8 is obtained, which provides an excellent match to the measured velocity profile. Good agreement is also obtained for experiment T, for which the A_b/k_n of 0.248 provides an A coefficient of 6.15 and a corresponding boundary layer thickness of 5.36 cm. Since the predicted velocity profiles match the measured velocity profiles, the *Madsen* [1984] model is shown to adequately characterize boundary layers for both spectral waves

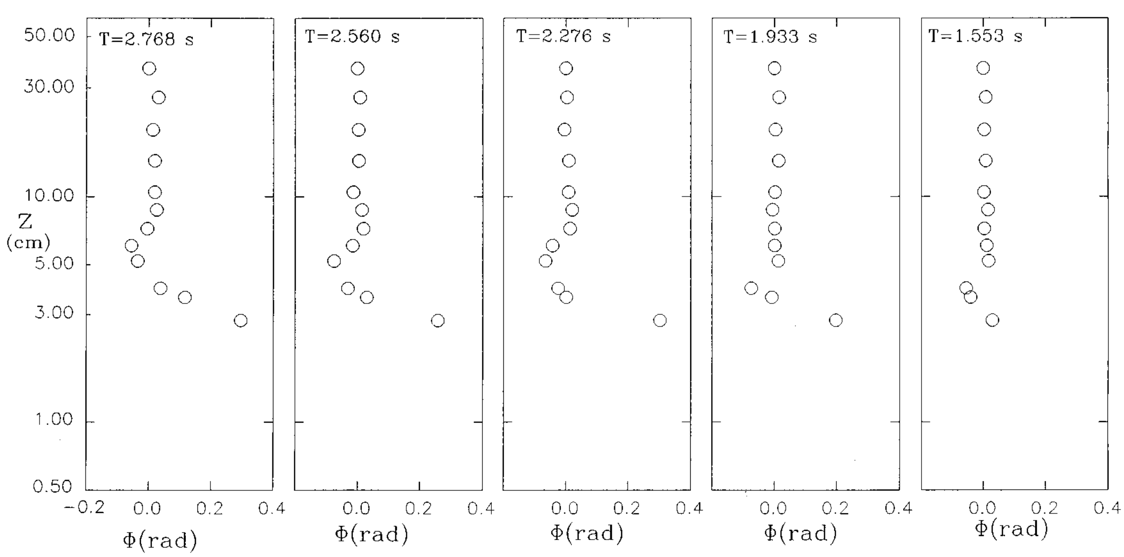

Figure 9. Profiles of wave velocity phase for all spectral wave components for experiment S, measured 9.5 m downstream of the current inlet.

and currents, provided its application includes an appropriate boundary layer thickness computed from (29) with the value of A obtained from *Madsen and Salles* [1999].

Mathisen and Madsen [1996b] also used the current shear velocity, u_{*c}, and apparent hydraulic roughness, z_{oa}, determined from measured velocity profiles as input to the *Grant and Madsen* [1986] model to obtain independent estimates for the bottom roughness experienced by the current in the presence of waves, k_{cw}. Following the procedures outlined by *Mathisen and Madsen* [1996b], the boundary layer thickness is set to the value determined from (29), and z_{oa} and u_{*c} are used in conjunction with the *Madsen* [1994] model to determine a hydraulic roughness z_o. This hydraulic roughness is then related to the bottom roughness since $z_o = k_{cw}/30$. Using this approach, the k_{cw} values for experiments S and T are determined to be 16.9 and 22.8 cm, respectively. These values closely match the corresponding k_{wc} values listed in Table 1 (17.5 and 18.0 cm, respectively). The close correspondence between k_{cw} and k_{wc}, which is a result of the excellent agreement between predicted and measured current velocity profiles, further demonstrates that the *Madsen* [1994] model, with the boundary layer thickness predicted using the results of *Madsen and Salles* [1999], characterizes currents as well as waves for combined wave-current flows.

Mathisen and Madsen [1996b] showed that wave-induced mass transport also could affect velocity profiles for currents in the presence of monochromatic waves. In those experiments, wave-induced mass transport was estimated at the edge of the boundary layer for waves in the presence of a current from experiments with no current present. Similarly, for the present experiments, time-averaged velocity profiles were also measured for pure spectral waves with no current present in order to estimate the magnitude of the wave-induced mass transport for spectral waves. These measurements indicated that the wave-induced mass transport at the edge of the wave boundary layer was less than 0.5 cm/s for the two different wave conditions, which is small relative to the time-averaged current velocity at the edge of the wave boundary layer. Since any effects of wave-induced mass transport are well within the accuracy of the apparent roughness determinations, it is concluded that wave-induced mass transport does not significantly affect current velocity profiles measured for these experiments. Therefore no correction is considered to be necessary to account for the effects of wave-induced mass transport for these experiments, and the *Madsen* [1994] model with modifications for an enhanced boundary layer thickness is considered to be sufficient to characterize velocity profiles for currents in the presence of spectral waves.

8. Summary and Discussion

Mathisen and Madsen [1996a, b] showed that a single roughness may be used to characterize pure currents, pure waves, and combined wave-current flows over the same bottom configuration. This paper extends these results to spectral waves by investigating the boundary layers for discrete wave spectra, consisting of five wave components, propagating over the same bottom configuration. Wave attenuation due to bottom friction was determined for individual wave components by accounting for the effects of sidewall dissipation and nonlinear energy transfers between different wave components. Using an equivalent wave representation defined by the root-mean-square horizontal near-bottom orbital velocity, these wave attenuation estimates were used in conjunction with conservation of wave energy to determine representative energy dissipation factors $f_{e,r}$. These $f_{e,r}$ values were then used as input to the model of *Madsen* [1994] to estimate bottom roughnesses experienced by the spectral waves in the presence and absence of a current. The roughness determinations agreed with similar roughness determinations for the monochromatic wave experiments completed by *Mathisen and Madsen* [1996a, b] in the same wave flume.

Once wave roughnesses were estimated, the representative wave was investigated for use as a predictive tool for determining wave attenuation. Experimentally determined bottom roughnesses, k_w and k_{wc}, and their associated representative energy dissipation factors, $f_{e,r}$, were used to predict attenuation for individual wave components. The use of energy dissipation factors, $f_{e,j}$, for individual wave components, as determined from the theory of *Madsen* [1994], was compared to the use of a single energy dissipation factor, $f_{e,j} = f_{e,r}$, for all wave components. Comparisons of predicted attenuation with measured attenuation showed that both approaches yield good agreement between predicted and measured attenuation. However, the predictions of the *Madsen* [1994] model provided a slightly improved agreement with measurements for experiments with lower intensity wave conditions, in that the variable friction factor reproduced an observed tendency of an increase of attenuation with increasing frequency.

Using the wave roughness determined from experimental data, the *Madsen* [1994] model was used to predict time-averaged current velocity profiles. Wave-induced mass transport was found to have a small effect on velocity profiles (and therefore the roughnesses) measured in these experiments, although additional research is necessary to define the role of wave-induced mass transport in field conditions involving spectral waves. In addition, the "enhanced boundary layer thickness" that was originally observed by *Mathisen and Madsen* [1996b] and is also observed in these experiments is now resolved analytically by modifying the model of *Madsen* [1994] to incorporate the boundary layer thickness obtained by *Madsen and Salles* [1999]. The velocity profiles predicted by the *Madsen* [1994] model closely matched the measured time-averaged velocity profiles for the current in the presence of waves, provided the wave boundary layer thickness was computed using the result of *Madsen and Salles* [1999].

In addition to verifying the use of a single roughness for spectral waves, these experiments also provide verification that the characteristics of the boundary layer for spectral waves may be represented using a single representative monochromatic wave of the form defined by (16) and (17). Comparisons between wave attenuation for individual wave components and predictions of wave attenuation afforded by the *Madsen* [1994] model demonstrate this model's ability to predict the distribution of spectral wave attenuation resulting from bottom dissipation. The success of the *Madsen* [1994] model in representing the experimental results additionally confirms the utility of using an equivalent wave representation as proposed by this model to characterize boundary layers for spectral waves in the presence and absence of a current. Since all data in the present study were analyzed using the *Madsen* [1994] model (with modifications to account for the presence of an enhanced boundary layer thickness), the use of a single roughness can be considered valid only when used in conjunction with this model.

While the details regarding the practical application of the

Madsen [1994] model (modified to incorporate the results of *Madsen and Salles* [1999]) can be found in those papers, it is appropriate to comment on the practical application of this model when detailed experimental data are not available. For instance, predictive models or field observations are often used to provide a surface wave spectrum, $S_{\eta\eta}(\omega)$, consisting of wave amplitudes, frequencies, and directions. For unidirectional waves and currents, the representative near-bottom velocity and radian frequency can be determined by converting this surface wave spectrum into a bottom orbital velocity spectrum, $S_{u_b u_b}(\omega)$, and making use of (16) and (17). With known current conditions and this definition for the spectrum, the only remaining parameter necessary to predict boundary layer characteristics and spectral wave attenuation is the bottom roughness. For a movable sediment bed, common practice is to assume a roughness that is 4 times the bed form height. *Madsen and Salles* [1999] used (24) to reanalyze available experimental data on the energy dissipation in wave bottom boundary layers over movable sediment beds and found that the roughness is more appropriately represented as $k_w = 12\eta$. For these experiments, the physical roughness height η for the triangular bars is 1.5 cm and the roughness values in Table 1 range from 9η to 18η. Consequently, a selection of $k_w = 12\eta$ is consistent with these experiments and provides a reasonable single-parameter relationship for estimating the roughness for a movable sediment bed. In practice, k_w could then be used in conjunction with (24) and (27) to determine the representative friction factor, $f_{wc,r}$, and individual friction factors for various wave components, $f_{wc,i}$. Attenuation for individual wave components can then be estimated from (20). Finally, for a codirectional wave-current flow, the same roughness is appropriate and the time-averaged velocity profile outside of the wave boundary layer takes the form of (26), with the wave boundary layer thickness defined by (29). If the current direction is at an angle to the wave direction, the characteristics of the energy dissipation and associated roughness change and the conclusions regarding wave-current interaction obtained in the present study may no longer be valid.

In any case, a major challenge is to obtain an appropriate estimate of the bed form geometry and bottom characteristics. The equivalent wave concept provides an approach that can simplify some of the complexities of fluid-sediment interaction to address this challenge. For example, the equivalent wave provides a basis for comparing extensive data sets from laboratory experiments using monochromatic waves to more realistic field conditions with spectral waves. *Madsen et al*. [1990] completed experiments for monochromatic and spectral waves propagating over movable sediment beds in the same flume as the one used for the present study. For those experiments, spectral wave roughnesses were determined to be lower than the monochromatic wave roughnesses. The present experiments provide confidence that the roughnesses for both monochromatic and spectral waves (represented in terms of an equivalent monochromatic wave) propagating over the same bottom configuration are essentially the same. This suggests that any differences between roughnesses for monochromatic and spectral waves can be attributed to differences between their respective bottom configurations. Therefore the results of the present investigation confirm that any discrepancies between monochromatic and spectral wave roughnesses observed in movable bed experiments should be attributed to differences in bed form characteristics associated with monochromatic and spectral waves.

Although the results presented in this paper verify that a single roughness scale and representative monochromatic wave can be used in conjunction with the *Madsen* [1994] model, some questions still remain. For example, *Mathisen and Madsen* [1996b] showed that wave-induced mass transport affected time-averaged velocity profiles for combined wave-current flows. Quantification of this wave-induced mass transport for the present experiments and previous experiments of *Mathisen and Madsen* [1996b] required experimental measurements of time-averaged velocity profiles for pure waves with no current present. Additional research is necessary to develop predictive tools for quantifying this wave-induced mass transport. Furthermore, the experimental conditions for the current investigation included codirectional waves and currents. Additional research is necessary to investigate the nature of the boundary layer and bottom roughness when the waves and current are in different directions. Thus the results presented in this paper provide a basis for these additional investigations to better understand the nature of bottom boundary layers and fluid-sediment interactions.

Appendix: Corrections to "Waves and Currents over a Fixed Rippled Bed" [*Mathisen and Madsen*, 1996a, b]

When completing the analyses presented in this paper, an approximation error was found in the software used to calculate wave roughnesses presented by *Mathisen and Madsen* [1996a]. While the graphical relationship shown by Figure 4 of *Mathisen and Madsen* [1996a] was accurately presented, an approximation error was found in the software used to represent this relationship in the calculations. Because of this unfortunate oversight, the roughnesses presented by *Mathisen and Madsen* [1996a, b] were slightly in error. However, this approximation error had only minor effects on the roughness magnitudes determined by *Mathisen and Madsen* [1996a, b], and all conclusions in these two papers remain the same.

To provide an accurate and complete summary of all roughnesses determined for the experiments conducted by *Mathisen and Madsen* [1996a, b], a summary table is included here as Table A1. This table follows the same format as Table 2 of *Mathisen and Madsen* [1996b], but it now includes more accurate values for the monochromatic wave roughnesses. As in the work by *Mathisen and Madsen* [1996b], roughness comparisons for the 20-cm spacing are considered to be inconclusive owing to the limited data available for this spacing. In addition, some variability is evident in the roughness estimates, although no specific trends can be identified. Roughnesses are therefore compared in terms of mean values. *Mathisen and Madsen* [1996b] listed geometric mean roughnesses of 22.8 cm for k_{cw}, 19.3 cm for k_{wc}, 23.5 cm for k_w, and 20.9 cm for k_c. Calculation of corrected geometric mean values for the 10-cm spacing yields 21.4 cm for k_{cw}, 16.3 cm for k_{wc}, 21.1 cm for k_w, and 20.9 cm for k_c. On the basis of these four roughness estimates, the geometric mean roughness is now 19.8 cm, which is slightly lower than the value of 21.4 listed by *Mathisen and Madsen* [1996b]. Each of the four roughness estimates is still within 15% of this mean roughness, which indicates an accuracy that is significantly better than our present ability to predict the bottom roughness for a movable sediment bed. This result leads us to the same conclusion as that of *Mathisen and Madsen* [1996b]; that is, the roughness experienced by the current in the presence of waves is the same as the roughnesses for pure

Table A1. Roughness Comparisons for Monochromatic Waves

Experiment	T, s	U, cm/s	A_b, cm	k_{cw}, cm	k_{wc}, cm	k_w, cm	k_c, cm
A	2.24	16	6.45	27.3	16.2	25.3	23.6
B	2.63	16	8.08	19.5	12.0	19.7	23.6
C	2.89	16	8.80	22.5	14.7	15.1	23.6
G	2.24	12	6.37	···	17.7	25.3	18.1
H	2.63	12	8.00	12.9	12.1	19.7	18.1
I	2.89	12	8.84	···	22.5	15.1	18.1
J	2.24	12	4.31	24.6	18.0	24.7	18.1
K	2.63	12	5.61	14.4	16.5	22.9	18.1
L	2.89	12	6.12	38.1	20.1	21.0	18.1
M[a]	2.24	16	6.61	···	7.8	7.2	···
N[a]	2.63	16	8.22	17.7	6.9	7.0	···
O[a]	2.89	16	9.11	···	8.4	4.8	···
P[a]	2.24	12	6.55	···	6.3	7.2	12.6
Q[a]	2.63	12	8.20	13.2	8.7	7.0	12.6
R[a]	2.89	12	9.18	···	13.5	4.8	12.6

[a]Experiments had a 20-cm roughness spacing.

currents, pure waves, and waves in the presence of a current for the same bottom configuration.

Acknowledgments. The research results presented in this paper expand upon the doctoral dissertation of Paul P. Mathisen, prepared under the guidance of Ole S. Madsen at Ralph M. Parsons Laboratory, Massachusetts Institute of Technology. Support for experiments conducted at Ralph M. Parsons Laboratory for this research was provided by the MIT Sea Grant College Program under grant NA90-AA-D-SG424 from the Office of Sea Grant, National Oceanic and Atmospheric Administration, U.S. Department of Commerce. Additional support was received from National Science Foundation's Marine Geology and Geophysics Program, grants OCE-9017878 and 9314366, and Ocean Sciences CoOP grant OCE-9123513.

References

Biésel, F., and F. Suquet, Les appareils générateurs de houle en laboratoire, *Houille Blanche*, *6*(2), 147–165, 1951.

Christoffersen, J. B., and I. C. Jonsson, Bed friction and dissipation in a combined wave and current motion, *Ocean Eng.*, *12*(5), 387–423, 1985.

Collins, J. I., Prediction of shallow-water spectra, *J. Geophys. Res.*, *77*(15), 2693–2707, 1972.

Graber, H. C., A parametric wind wave model for arbitrary water depths, Sc.D. thesis, Mass. Inst. of Technol., Cambridge, 1984.

Grant, W. D., and O. S. Madsen, Combined wave and current interaction with a rough bottom, *J. Geophys. Res.*, *84*(C4), 1797–1808, 1979.

Grant, W. D., and O. S. Madsen, The continental shelf boundary layer, *Annu. Rev. Fluid Mech.*, *18*, 265–305, 1986.

Hasselmann, K., On the non-linear energy transfer in a gravity wave spectrum, 1, General theory, *J. Fluid Mech.*, *12*, 481–500, 1962.

Hasselmann, K., and J. I. Collins, Spectral dissipation of finite depth gravity waves due to turbulent bottom friction, *J. Mar. Res.*, *26*(1), 1–12, 1968.

Hasselmann, K., et al., Measurements of wind-wave growth and swell decay during the Joint North Sea Wave Project (JONSWAP), *Dtsch. Hydrogr. Z.*, *12*, 1–95, 1973.

Hunt, J. N., Viscous damping of waves, *Houille Blanche*, *7*, 836–852, 1952.

Jonsson, I. G., Wave boundary layers and friction factors, in *Proceedings of the 10th Conference on Coastal Engineering*, pp. 127–148, Am. Soc. of Civ. Eng., New York, 1966.

Kajiura, K., A model of the bottom boundary layer in water waves, *Bull. Earthquake Res. Inst. Univ. Tokyo*, *46*, 75–123, 1968.

Kitiagorodskii, S. A., V. P. Krasitskii, and M. M. Zaslavaskii, On Phillips theory of equilibrium range in the spectra of wind-generated gravity waves, *J. Phys. Oceanogr.*, *5*, 410–420, 1975.

Lundgren, H., Turbulent currents in the presence of waves, in *Proceedings of 13th International Conference on Coastal Engineering*, pp. 623–634, Am. Soc. of Civ. Eng., New York, 1972.

Madsen, O. S., Spectral wave-current bottom boundary layer flows, in *Proceedings of the 24th International Conference on Coastal Engineering*, pp. 384–398, Am. Soc. of Civ. Eng., New York, 1994.

Madsen, O. S., and P. Salles, Eddy viscosity models for wave boundary layers, in *Proceedings of the 26th International Conference on Coastal Engineering*, pp. 2615–2627, Am. Soc. of Civ. Eng., New York, 1999.

Madsen, O. S., Y.-K. Poon, and H. C. Graber, Spectral wave attenuation by bottom friction: Theory, in *Proceedings of the 21st International Conference on Coastal Engineering*, pp. 492–504, Am. Soc. of Civ. Eng., New York, 1988.

Madsen, O. S., P. P. Mathisen, and M. M. Rosengaus, Movable bed friction factors for spectral waves, in *Proceedings of the 22nd International Conference on Coastal Engineering*, pp. 420–429, Am. Soc. of Civ. Eng., New York, 1990.

Mathisen, P., Experimental study on the response of fine sediments to wave agitation and associated wave attenuation, M.S. thesis, Mass. Inst. of Technol., Cambridge, 1989.

Mathisen, P., Bottom roughness for wave and current boundary layers over a rippled bed, Ph.D. thesis, Mass. Inst. of Technol., Cambridge, 1993.

Mathisen, P., and O. S. Madsen, Bottom roughness for waves and current boundary layer flows over a rippled bed, *Sea Grant Rep. MITSG 93-27*, Sea Grant Coll. Program, Mass. Inst. of Technol., Cambridge, 1993.

Mathisen, P., and O. S. Madsen, Waves and currents over a fixed rippled bed, I, Bottom roughness experienced by waves in the presence and absence of a current, *J. Geophys. Res.*, *101*(C7), 16,533–16,542, 1996a.

Mathisen, P., and O. S. Madsen, Waves and currents over a fixed rippled bed, 2, Bottom and apparent roughness experienced by currents in the presence of waves, *J. Geophys. Res.*, *101*(C7), 16,543–16,550, 1996b.

Rosengaus, M., Experimental study on wave generated bedforms and resulting wave attenuation, Ph.D. thesis, Mass. Inst. of Technol., Cambridge, 1987.

Smith, J. D., Modeling of sediment transport on continental shelves, in *The Sea*, vol. 6, edited by E. D. Goldberg et al., pp. 538–577, John Wiley, New York, 1977.

Tanaka, H., and N. Shuto, Friction coefficient for a wave-current coexisting system, *Coastal Eng. Jpn.*, *24*, 105–128, 1981.

U.S. Army Coastal Engineering Research Center, *Shore Protection Manual*, vols. I–III, 4th ed., U.S. Gov. Print. Off., Washington, D. C., 1984.

O. S. Madsen, Ralph M. Parsons Laboratory, Department of Civil and Environmental Engineering, Massachusetts Institute of Technology, 77 Massachusetts Avenue, Cambridge, MA 02139. (osm@mit.edu)

P. P. Mathisen, Department of Civil and Environmental Engineering, Worcester Polytechnic Institute, 100 Institute Road, Worcester, MA 01609. (mathisen@wpi.edu)

(Received June 26, 1997; revised August 14, 1998; accepted October 23, 1998.)